To cross or not to cross: Collective swimming of Escherichia coli under two-dimensional confinement

Dipanjan Ghosh * and Xiang Cheng *

Department of Chemical Engineering and Materials Science, University of Minnesota, Minneapolis, Minnesota 55455, USA



(Received 27 October 2021; accepted 20 April 2022; published 9 May 2022)

Bacteria suspended in fluids swim collectively and display fascinating emergent dynamics. Although bacterial collective swimming in bulk suspensions has been well studied, its counterpart in confined two-dimensional (2D) geometries relevant to many natural habitats of bacteria is still poorly understood. Here, through carefully designed experiments on *Escherichia coli* in a Hele-Shaw geometry, we show that a small change in the degree of confinement leads to a drastic change in bacterial collective swimming. While a long-range nematic order emerges for bacteria that can cross over each other during encounters, a slight decrease of the confining height that prevents the crossing leads to the formation of bacterial clusters with a short-range polar order. By tracking the swimming kinetics of individual bacteria, we reveal the microscopic origins of the two emergent collective phases and illustrate the effect of the collective dynamics on the swimming behaviors of single bacteria. Our study provides insights into bacterial collective swimming under confinement and demonstrates a simple way to control the emergent symmetry of collective phases.

DOI: 10.1103/PhysRevResearch.4.023105

I. INTRODUCTION

Collective motion of bacteria epitomizes the emergent dynamics of active matter [1–4], which leads to unusual transport properties of bacterial suspensions and confers upon bacteria evolutionary advantages crucial for their survival [5,6]. The natural habitats of bacteria often consist of confined spaces such as thin biofilms on solid substrates [7], pores of the soil [8,9], and the interstitial confines of tissues [10]. Consequently, understanding the collective dynamics of bacteria in confined systems is vital for deciphering various life-supporting activities of bacteria. However, although the collective swimming of bulk bacterial suspensions—the so-called "bacterial turbulence"—have been extensively studied in recent years [11–16], our understanding of the collective dynamics of bacterial suspensions under geometric confinement is still primitive.

In addition to the broad biological relevance, uncovering the collective dynamics of bacteria in confined geometries would provide insights into the emergent behavior and symmetry of active matter in reduced dimensions. While the long-range hydrodynamic interaction plays a leading role in inducing bacterial turbulence in bulk samples [15], both the nature and strength of the interaction are strongly modified in confined systems. Particularly, for bacteria confined between two rigid walls, the far-field flow generated by a swimming bacterium has the signature of a source dipole [17,18], qualitatively different from the well-known force dipole flow in a 3D

Published by the American Physical Society under the terms of the Creative Commons Attribution 4.0 International license. Further distribution of this work must maintain attribution to the author(s) and the published article's title, journal citation, and DOI.

bulk fluid. More importantly, the short-range steric interaction that is inconsequential in 3D suspensions becomes essential in mediating the collective dynamics of bacteria in confined systems [19,20]. These qualitative changes of interbacterial interactions result in novel collective phases of bacterial suspensions in confined systems [21–23], which cannot persist in 3D bulk suspensions.

Inspired by different confined geometries in nature, several different types of confinement have been experimentally implemented. Extending early works on bacterial turbulence in bulk samples [11-13], weak 3D confinement has been imposed by either narrow microfluidic channels or small droplets [24-27]. The weak confinement rectifies the chaotic turbulent flow of collective bacterial swimming into persistent unidirectional flow. Interbacterial interactions are qualitatively changed when a stronger confinement is applied to bacterial suspensions. In contrast to the long-range hydrodynamic interactions that govern bacterial turbulence [15], steric and/or short-range hydrodynamic interactions dictate the local alignment of cell bodies in a monolayer of swarming bacteria confined to the surface of an agar plate, which lead to various 2D phases of different swarming patterns [23,28– 30]. The agar geometry possesses a stress-free air-fluid interface, therefore relaxing the degree of confinement from the perspective of hydrodynamics. More recently, the strict 2D confinement has also been studied, where bacteria are confined in a Hele-Shaw cell between two rigid walls [21,22]. Using elongated filamentous cells of Escherichia coli (E. coli), Nishiguchi et al. reported the emergence of collective bacterial swimming with long-range nematic order in the Hele-Shaw geometry [21]. In contrast, Swiecicki et al. observed the formation of bacterial clusters with local polar order in a similar geometry [22]. Why do similar experiments yield collective phases with qualitatively different symmetries? How does confinement modify the interbacterial interactions and affect the alignment of

^{*}ghosh135@umn.edu

[†]xcheng@umn.edu

collectively swimming bacteria? We aim to address these questions in our study.

Our study focuses on bacterial suspensions under strong 2D confinement in the Hele-Shaw geometry. We find that the alignment of collectively swimming bacteria is sensitive to the degree of confinement. A small variation in the gap thickness between two rigid walls can trigger a drastic change of the collective behaviors of bacteria and yield emergent phases of qualitatively different symmetries. The finding resolves the controversy surrounding the contradictory observations on bacterial dynamics under confinement from previous experiments. Our study further reveals that the origin of the different collective phases is directly related to the microscopic interbacterial interaction. While bacteria that can cross over each other during close encounters form long-range nematic order, bacteria that are strictly constrained into a single layer under slightly tighter confinement assemble into transient clusters with local polar order. Hence, a subtle change in the interbacterial interaction has a profound effect on the emergent collective bacterial dynamics. Lastly, we show that the binary interaction between bacteria always favors nematic alignment, independent of the degree of confinement. Instead, the polar order of bacterial clusters arises from many-body steric interactions enabled by the noncrossing encounters between bacteria under strong confinement. These many-body interactions result in abnormally short swimming persistence and large velocity fluctuations of bacteria in the cluster phase. Taken together, our experiments on confined bacterial suspensions provide an excellent example illustrating the generic relation between the local particle interaction and the global symmetry of emergent collective phases in active matter. Our study further demonstrates geometric confinement as an effective tool to control the collective dynamics of bacterial suspensions, paving a way to engineer the swimming behaviors of bacteria in technical applications.

II. EXPERIMENT

In our experiments, we use genetically modified lightpowered E. coli (Appendix A 1), whose swimming velocity V can be continuously varied by changing the intensity of incident light [15,16]. At the maximum light intensity adopted in our experiments, the average swimming velocity of bacteria is $V = 13.3 \pm 2.5 \ \mu \text{m/s}$ in the dilute limit. The standard deviation of the normalized swimming velocity of individual bacteria over time is 0.25. The length and the width of bacterial bodies are $3.4 \pm 0.7 \ \mu m$ and $0.9 \pm 0.1 \ \mu m$, respectively. The aspect ratio of the bodies is 3.8 ± 1.2 . This body geometry is the same as that of wild-type E. coli strains. In addition to bacterial swimming velocity, we also vary 2D bacterial number density *n* between 1.1×10^6 up to 2.2×10^7 mm⁻². Above 2.2×10^7 mm⁻², bacteria become immotile in our confined system, possibly due to the intertwining of flagellar bundles at high densities.

We confine a suspension of *E. coli* of controlled volume in a Hele-Shaw chamber made of a glass slide and a coverslip (Appendix A 2). The lateral dimension of the chamber is fixed at 18 mm by 18 mm, whereas the gap thickness of the chamber is controlled by the volume of the suspension. We test two different suspension volumes, $0.7 \mu L$ and $0.9 \mu L$,

in our experiments. As the suspension is completely confined underneath the coverslip by capillary forces, the gap thickness is fixed at $h \approx 2.2~\mu m$ for the small-volume suspension and $h \approx 2.8~\mu m$ for the large-volume suspension. Thus, the gap thicknesses of the small-volume and large-volume chambers are approximately twice and three times of the average bacterial body width, respectively. The chamber is finally sealed on all sides by a UV-curable adhesive, which eliminates the influence of ambient airflow on the bacterial motion. To prevent bacteria from sticking on glass surfaces, glass slides and coverslips are base washed with 1 M NaOH before use.

Bacteria in the chamber are then imaged using an inverted bright-field microscope at a frame rate of 30 fps for 1000 frames with a field of view of 251 μ m by 225 μ m (Appendix A3). By postprocessing the resulting images (Appendix A 4), we identify the position \mathbf{r} and the orientation θ of bacterial bodies along the direction of their swimming and the instantaneous velocity v of bacteria. For a given bacterium i, we analyze the temporal variation of its velocity $v_i(t)$. The time-average velocity of the bacterium over its trajectory is $\langle v_i \rangle = T^{-1} \int_0^T v_i(t) dt$, where T is the total time duration of the trajectory within the field of view. By averaging $\langle v_i \rangle$ over all bacteria in a video, we obtain the ensemble average bacterial velocity $V = N^{-1} \sum_{i=1}^{N} \langle v_i \rangle$, where N is the total number of bacteria in the video. Finally, the instantaneous area fraction of bacteria is defined as the ratio of the number of pixels occupied by bacteria to the total number of pixels in the frame of a video. The time-averaged area fraction ϕ is then calculated by averaging over all the frames of the video. ϕ is proportional to the number density of bacteria n via $\phi = nA$, where A is the average cross-section area of bacteria in the 2D plane.

III. RESULTS

A. Collective swimming in 2D and quasi-2D geometries

With the small change of the gap thickness, we observe two qualitatively different collective phases of bacterial suspensions under confinement, which are characterized by different orientational orders of bacteria. When the gap thickness is large, a case we shall refer to as the quasi-2D geometry below, bacteria show random motions at low densities ϕ and small bacterial swimming velocities V. With increasing ϕ and V, bacteria tend to align nematically over a long range. At high ϕ and V, the collective motion of bacteria shows a clear long-range nematic order, where bacterial bodies align along a preferred direction with bacteria themselves swimming either parallel or antiparallel along the direction [Figs. 1(a) and 1(b)] (also Movie 1 in the Supplemental Material [31]). We quantify the strength of the nematic alignment using the order parameter $S = (\langle \cos 2\theta \rangle^2 + \langle \sin 2\theta \rangle^2)^{1/2}$ [Fig. 1(c)], where $\langle \cdot \rangle$ indicates an average over all the bacteria in the field of view. S = 1 indicates a perfect alignment, whereas S = 0 for random orientations. Consistent with our direct observation, S is small at low ϕ and V. Bacterial dynamics are dominated by Brownian motions at low V, which disrupt long-range orientational order and result in small S. S increases with ϕ and V and reaches S = 0.7 at high ϕ and V. The long-range nematic phase has been reported in experiments with filamentous cells

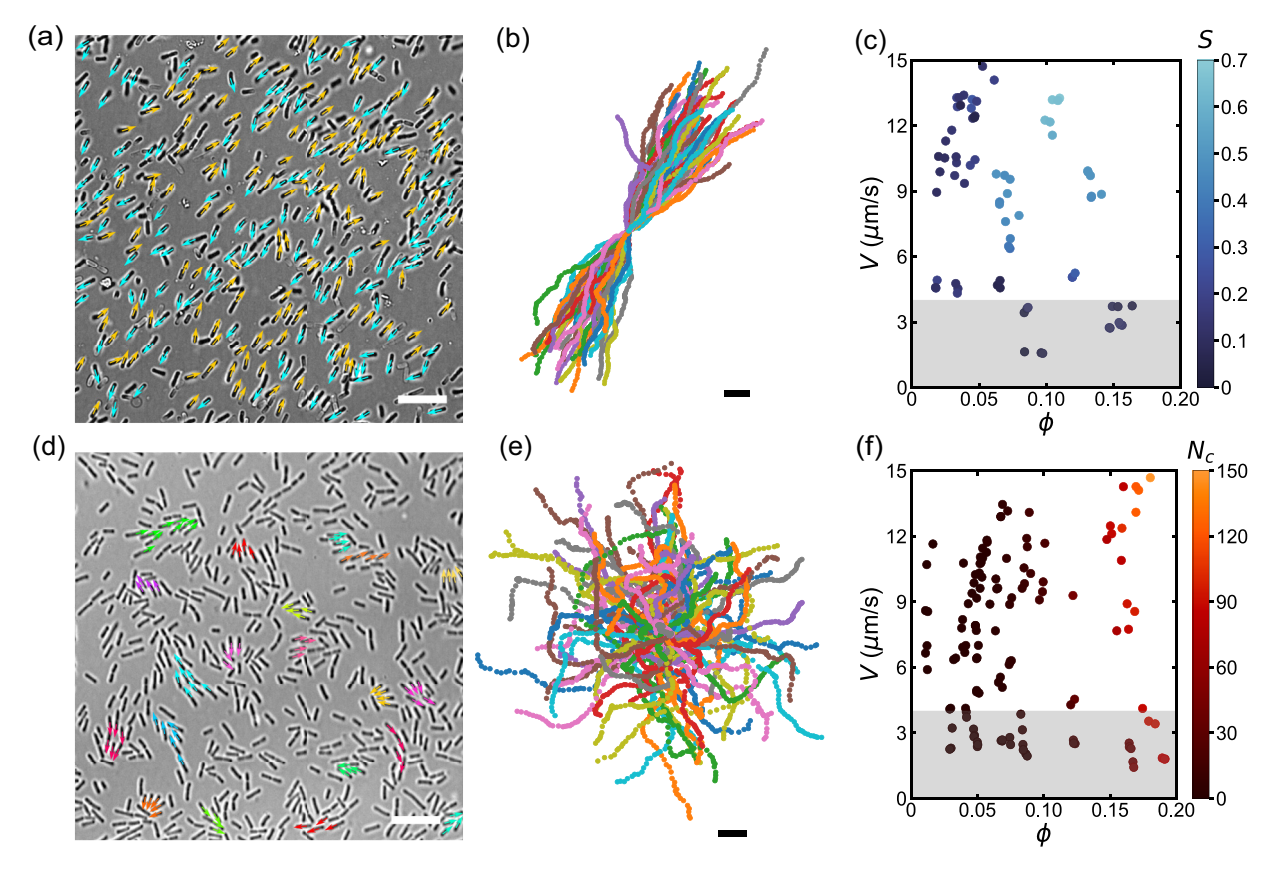


FIG. 1. Collective swimming of *E. coli* in the quasi-2D (top row) and 2D (bottom row) geometries. (a) Microscopy image of a bacterial suspension in the quasi-2D geometry exhibiting a long-range nematic order. The gold and cyan arrows indicate the direction of bacterial swimming, showing the two directions along which bacteria are predominantly oriented. (b) Representative trajectories of bacteria in the quasi-2D geometry, with the starting point of each trajectory translated to a single point at the center. The preferred orientations of the trajectories illustrate the nematic order of bacteria. (c) Phase diagram showing the dependence of the nematic order parameter *S* on the bacterial swimming velocity *V* and area fraction ϕ . (d) Microscopy image of a bacterial suspension in the 2D geometry exhibiting bacterial clusters with a short-range polar order. Arrows of different colors are used to mark different clusters. (e) Representative trajectories of bacteria in the 2D geometry, with the starting point of each trajectory translated to a single point at the center. (f) Phase diagram showing the dependence of the number of clusters N_c in the field of view on *V* and ϕ . The gray regions in (c) and (f) correspond to slow and randomly moving bacteria with velocities below 4 μ m/s under light of low intensities. Scale bars are 10 μ m.

of *E. coli* with a large aspect ratio of bacterial bodies \sim 25 [21]. Our experiments show that under strong confinement, a long-range nematic order can also arise in normal-size bacteria with an aspect ratio of \sim 4.

For the small gap thickness, a case we shall refer to as the 2D geometry below, bacteria also show random motions at low ϕ and small V, similar to those in the quasi-2D geometry. Nevertheless, with increasing ϕ and V, instead of the long-range nematic order, bacteria form transient clusters with a short-range polar order [Fig. 1(d)] (also Movie 2 in Supplemental Material [31]). Such structures have been termed as "bacterial rafts" by Swiecicki et al [22]. The trajectories of individual bacteria in 2D are much less persistent than those in quasi-2D, without a clear sign of nematic alignment [Fig. 1(e)]. To characterize the collective behavior in the 2D geometry, we assign bacteria into clusters based on the distance between them and the difference between their orientations [30,32]. A pair of bacteria are adjacent neighbors when the distance between the centroids of their bodies $\Delta r \equiv |\mathbf{r_1} - \mathbf{r_2}| < 3 \,\mu\mathrm{m}$ and the difference between their body orientation $\Delta\theta$ < 30°. Here, $\mathbf{r_1}$ and $\mathbf{r_2}$ are the centroids of the bodies of the two bacteria, respectively. A cluster is then defined as a group of bacteria where each bacterium belonging to the group is an adjacent neighbor with at least one other bacterium from the same group. Furthermore, a cluster must consist of at least 4 bacteria. We quantify the extent of cluster formation by counting the number of bacterial clusters N_c in our field of view. N_c increases with both ϕ and V and reaches $N_c = 150$ at high ϕ and V [Fig. 1(f)]. The qualitative feature of the phase diagram in Fig. 1(f), namely, the increase in N_c with ϕ , does not change when we vary the cut-off distance Δr and the cut-off angle $\Delta \theta$ within a reasonable range (Appendix A 5).

B. Binary collisions favor weak nematic alignment in both geometries

Why does a small change in the gap thickness lead to such a drastic change in the collective dynamics of bacteria? To answer this question, we first examine the pairwise interaction between bacteria at low ϕ and large V in both the quasi-2D and 2D geometries. Specifically, we analyze experiments

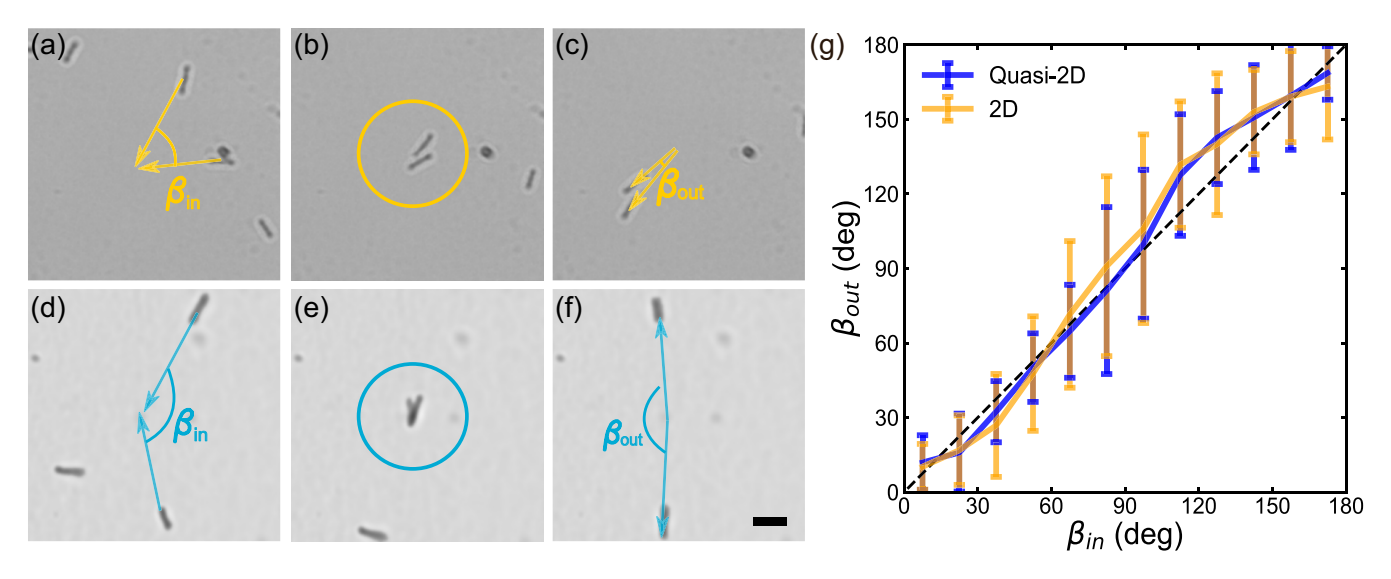


FIG. 2. Nematic alignment induced by binary collisions. [(a)–(c)] The time-lapse frames of a collision of two bacteria in the 2D geometry with an acute incoming angle β_{in} at t=-1, 0, and 1 s. [(d)–(f)] The time-lapse frames of a collision of two bacteria in the quasi-2D geometry with an obtuse β_{in} at t=-1, 0, and 1 s. Bacteria overlap in (e), illustrating a crossing event during the collision. Arrows indicate the direction of bacterial swimming. Scale bar in (f) is 5 μ m. (g) The outgoing angle β_{out} vs the incoming angle β_{in} for the quasi-2D (blue) and 2D (gold) geometries. A total of 1,119 collisions for quasi-2D geometry and a total of 1,287 collisions for the 2D geometry have been analyzed. The data are binned into 15° intervals of β_{in} . The blue and gold lines connect the means of β_{out} . The error bars indicate standard deviations. The black-dashed line represents the condition $\beta_{in} = \beta_{out}$, corresponding to collisions without any alignment. The detailed distributions of β_{in} and β_{out} are shown in Appendix B 1.

in the dilute limit with $\phi = 0.05$ and high bacterial activity $V = 13 \ \mu \text{m/s}$. A collision event between a pair of bacteria is again defined when the shortest distance between the two bacteria $\Delta r < 3 \mu m$. Under 2D confinement, the motion of a bacterium is influenced by the short-range hydrodynamic interaction with its neighbor within a distance equal to their cell body length [33], which justifies our choice of 3 μ m as the cut-off length for a collision event. The positions of the bacterial bodies are then tracked starting from 1 second before the collision event to 1 second after the collision event. Bacteria typically swim a distance of at least one cell-body length from their point of collision in 1 second, which is sufficient to determine their new direction of motion after a collision. We ensure collisions are strictly binary by excluding any collision event where a third bacterium gets within a distance of 6 μ m of either of the colliding bacteria during any instant of the collision event. The angle subtended by the positions of the two bacteria before the collision is termed the incoming angle β_{in} , whereas the angle subtended by their positions after the collision is called the outgoing angle β_{out} [Figs. 2(a)–2(f)].

Figure 2(g) shows β_{out} as a function of β_{in} for the quasi-2D and 2D geometries. Surprisingly, even though the emergent collective phases are qualitatively different, the binary interactions between bacteria are quantitatively similar in the two geometries. For acute incoming angles, the outgoing angle is slightly decreased, indicating a tendency for weak polar alignment, whereas, for obtuse incoming angles, a slight increase in the outgoing angle captures weak antipolar alignment. Thus, the binary interactions of bacteria in both the quasi-2D and 2D geometries favor a weak nematic symmetry [21,34–36], without any discernible bias towards polar alignment [37]. At high densities in the quasi-2D geometry at which the nematic order is observed, a bacterium undergoes multiple

successive binary collisions with its neighbors. Even though a single collision imparts only weak nematic alignment, the alignment resulting from multiple collisions is sufficient to induce long-range nematic order. However, the difference in the collective behaviors in the two geometries, particularly, the rise of bacterial clusters with the local polar order in 2D, cannot be explained by binary collisions.

C. To cross or not to cross

A detailed examination of bacterial dynamics at both low and high ϕ reveals a key difference in bacterial interactions in the quasi-2D and 2D geometries. While bacteria can cross over each other during a collision in the quasi-2D geometry [Fig. 2(e)], we do not observe bacterial crossing in the 2D geometry [Fig. 2(b)]. The tighter confinement of the 2D geometry strictly constrains bacteria to a single layer. The observation thus suggests that decreasing the thickness of the Hele-Shaw chamber, thereby switching off the ability of bacteria to cross over, drastically alters their emergent collective swimming behaviors.

While $0.7~\mu L$ drops form the 2D chamber and $0.9~\mu L$ drops give the quasi-2D chamber, using an intermediate drop size between 0.7 and $0.9~\mu L$ results in either a quasi-2D chamber or a 2D chamber. If the gap thickness of the chamber is sufficient for a pair of bacteria to cross during a collision, the resulting chamber is quasi-2D, which gives rise to the long-range nematic order. Otherwise, bacteria are confined to a monolayer and the chamber is 2D, which results in transient bacterial clusters with the local polar order. No intermediate cases are observed in our experiments. The ability of bacteria to cross is fixed globally by the gap thickness of confined geometries in our experiments. At a given gap thickness, the

collective swimming behavior of bacteria does not switch between nematic and polar states either spatially or temporally. Furthermore, the ability of bacteria to cross over each other is governed solely by the thickness of the chamber and is independent of the total number of bacteria in the chamber.

The relation between the emergent order of collective phases and the ability of individual active particles to cross during collisions has also been observed in other 2D active matter systems. In numerical simulations of active rods, the crossover between two particles can be controlled by the strength of the repulsive interparticle potential and the selfpropulsion speed of active particles [38]. For soft potentials at high speeds, a condition where particles can overlap and cross over each other, the symmetry of the emergent collective phase is nematic [36,39-41]. In contrast, slower speeds and stiffer repulsive potentials lead to noncrossing interparticle interaction and give rise to polar clusters [36,40,42] and bands [43,44]. A recent experiment with a 2D motility assay of microtubules has also shown that a nematic order emerges when the microtubules are able to cross over each other, whereas polar clusters form when they are unable to cross [34]. In this experiment, the ability of microtubules to cross was controlled by the density of motor proteins fixed on substrates. A low motor-protein density gives more flexibility to the tip of a microtubule and allows it to climb over other microtubules during a collision. In combination with these previous numerical and experimental findings, our experiments with swimming bacteria—a premier example of active matter—provide strong evidence illustrating a universal feature of 2D active matter: the ability of active particles to cross dictates the symmetry of emergent collective phases. Rather than modifying the properties of individual active particles, our study further demonstrates that geometric confinement can be used as a simple and effective tool to control the crossing ability of active particles and manipulate the collective dynamics of 2D active matter.

D. The rise and fall of bacterial clusters

While the long-range nematic order of bacteria in the quasi-2D geometry stems from the binary collision of bacteria in the dilute limit [Fig. 2(g)], bacterial clusters with the local polar order in the 2D geometry must arise from the many-body interactions enabled by the noncrossing collision at high densities [35,45].

To understand the origin of bacterial clusters, we image the dynamics of cluster formation in the 2D geometry. Specifically, we analyze 17 representative bacterial clusters from 3 independent experimental runs, each having a time-averaged bacterial area fraction $\phi = 0.15$. Each cluster contains 4–9 bacteria, giving a total of 117 bacteria across all of the clusters. The time instant when the members of a bacterial cluster are spatially closest to each other, quantified by a minimization of the sum of their pairwise distances, is assigned as the reference time t = 0. The positions and orientations of bacteria in these clusters are then tracked from t = -3 to 3 s at 0.1 s intervals. At each time step, we calculate the difference between the angles of adjacent neighbors $\Delta\theta_{ij}$, as well as the pairwise distances between all the members of a bacterial cluster Δr_{ij} [see the schematic in the inset of

Fig. 3(a)]. Figures 3(a) and 3(b) show Δr_{ij} of all bacterial pairs and $\Delta \theta_{ij}$ of all adjacent pairs of bacteria in the 17 bacterial clusters as a function of time. From t=-3 to 0 s, both the extents of Δr_{ij} and $\Delta \theta_{ij}$ decrease, indicating bacteria coming together and aligning to form a cluster. Subsequently, Δr_{ij} and $\Delta \theta_{ij}$ increase with time from t=0 to 3 s, showing the gradual dissolution of the clusters over time and revealing the transient nature of bacterial clusters in the 2D geometry. Qualitatively similar dynamic features are also observed at other area fractions (Appendix B 2).

Along with Δr_{ij} and $\Delta \theta_{ij}$, we also measure the normalized velocity of individual bacteria in the process of cluster formation and dissolution, $v/\langle v \rangle$. Here, v is the instantaneous velocity of a given bacterium and $\langle v \rangle$ is the time-averaged velocity of that particular bacterium. Figure 3(c) shows the time evolution of $v/\langle v \rangle$ averaged over all the bacteria in clusters. Around t = 0, $v/\langle v \rangle$ decreases substantially about 15% below its temporal average, suggesting an instantaneous slowing down at the instant of cluster formation. The forward motion of a bacterium can be partially blocked by neighboring bacteria that act as obstacles [32,35]. If multiple bacteria encounter the same obstacle, their velocities slow down simultaneously, which leads to the formation of a bacterial cluster. Each bacterium in the cluster further aligns with its neighbors, giving rise to local polar order [35,36]. If the bacterium aligned antiparallel with its neighbors, it would simply slide away without joining the cluster. Since a bacterium can cross past its neighbors in the third dimension, the collision-induced slowdown—the key feature underlying the cluster formation—does not occur in the quasi-2D geometry. As the mechanism of collision-induced slowdown requires the presence of multiple neighbors, the clustering does not occur at low ϕ either. Even though the two bacteria undergoing a collision slow down temporarily, there are few neighboring bacteria at low ϕ that can join the pair before they separate.

The increase in pairwise distances [Fig. 3(a)] and in adjacent angle differences [Fig. 3(b)] after t=0 suggest that the bacterial clusters in the 2D geometry are transient. Due to their short lifetimes, clusters are unable to grow and remain small in size. We verify this by measuring the size s_c of the observed clusters at different densities for a high bacterial velocity of $V=13 \mu \text{m/s}$. Figure 3(d) shows the probability distribution functions of s_c , $P(s_c)$. Bacteria are more probable to form large clusters at high ϕ , resulting in the slow decay of the tail of $P(s_c)$. However, even at high ϕ , the maximum cluster size is only $\sim \mathcal{O}(10)$, while the number of bacteria in the field of view is on the order of 10^3 . Thus, unlike the long-range nematic order that is formed by all bacteria in the field of view, the polar clusters are short-range and spatially localized.

Bacteria in the 2D geometry form clusters as their forward motion is being partially blocked by a common obstacle, which can be easily identified in most of the clusters in Fig. 1(c). When this obstacle moves away, the velocities of the bacteria in the cluster increase, as shown in Fig. 3(c) after t = 0. Figure 3(a) further shows that the pairwise distances between the bacteria in a cluster increase after t = 0, implying that the members of the cluster are moving apart. Such a phenomenon is possible when the swimming speed of a bacterium in a cluster depends on its relative position in the cluster. For example, if a bacterium that did not have any

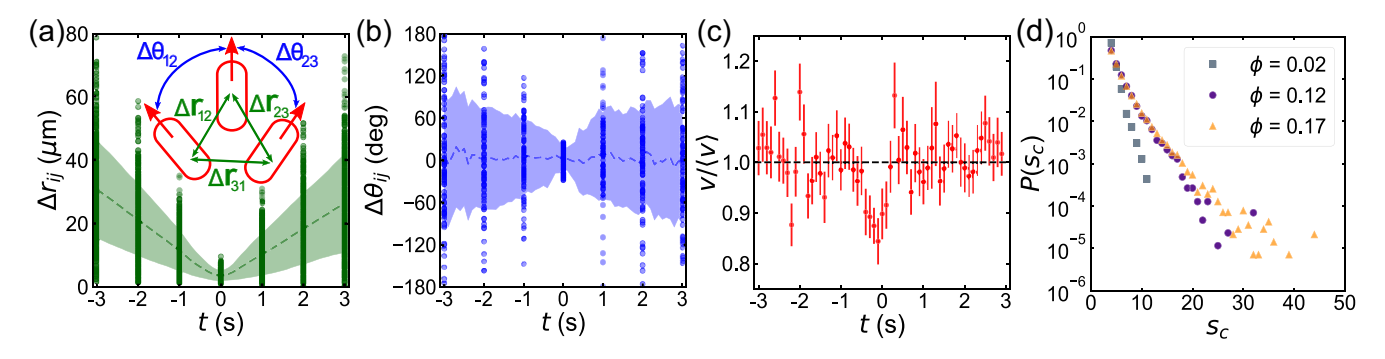


FIG. 3. Transient dynamics of bacterial clusters in the 2D geometry. (a) and (b) The time evolution of the pairwise distance Δr_{ij} and the adjacent angles $\Delta \theta_{ij}$ of bacterial clusters. The definition of Δr_{ij} and $\Delta \theta_{ij}$ between three neighboring bacteria are shown in the inset of (a). Disks are the data. To avoid crowding, we only show the data at the integer time of t=-3,-2,-1,0,1,2, and 3 s. The real measurements are conducted with the time resolution of $\Delta t=0.1$ s. The dashed line represents the mean of the data, whereas the shaded region indicates one standard deviation around the mean. Bacterial area fraction $\phi=0.15$. $\Delta r_{ij}(t)$ and $\Delta \theta_{ij}(t)$ at other ϕ s are shown in Appendix B 2. (c) The time evolution of the normalized velocity of bacteria $v/\langle v \rangle$ averaged over all the bacteria in clusters. The error bars represents the standard errors. The black-dashed line corresponds to the temporal average $v/\langle v \rangle=1$. (d) The probability distribution of the size of clusters s_c in the 2D geometry, $P(s_c)$, at $\phi=0.02$ (gray squares), $\phi=0.12$ (purple circles), and $\phi=0.17$ (gold triangles).

neighbors ahead of it swam faster than its neighbors, it could quickly move away from the cluster. The difference in the relative velocities of the bacteria in a cluster promotes the disintegration of the cluster and is ultimately responsible for the transient nature and the small size of bacterial clusters.

To probe the dependence of the swimming velocity of bacteria on their relative positions with respect to their neighbors, we measure the velocity of bacteria as a function of the distances of the bacteria to their closest neighbors. Specifically, at each time step, we identify the positions of the nearest Voronoi neighbors of the bacterium under consideration and calculate the distances between the bacterium and its nearest neighbors. We distinguish two types of neighbors. Neighbors lying within 45° of the swimming direction of the bacterium are identified as forward neighbors, whereas neighbors lying

within 45° of the opposite direction of the swimming are identified as backward neighbors [Fig. 4(a)]. The distance between the tracked bacterium and its forward nearest neighbor is termed r_f and the distance to its backward nearest neighbor is termed r_b . We examine the dependence of the normalized velocity of the bacterium $v/\langle v \rangle$ on r_f and r_b . To avoid the influence of the intrinsic variation of the swimming speed of bacteria, we consider only the cases with large velocity fluctuations, where bacterial velocity v is at least 30% above or below the mean.

Figures 4(b) and 4(c) show the joint plot of $v/\langle v \rangle < 0.7$ and $v/\langle v \rangle > 1.3$ as a function of r_f and r_b , respectively. For the slowdown events with $v/\langle v \rangle < 0.7$, most data cluster around lower values of r_f , where the forward nearest neighbors are at close distances [Fig. 4(b)]. The observation

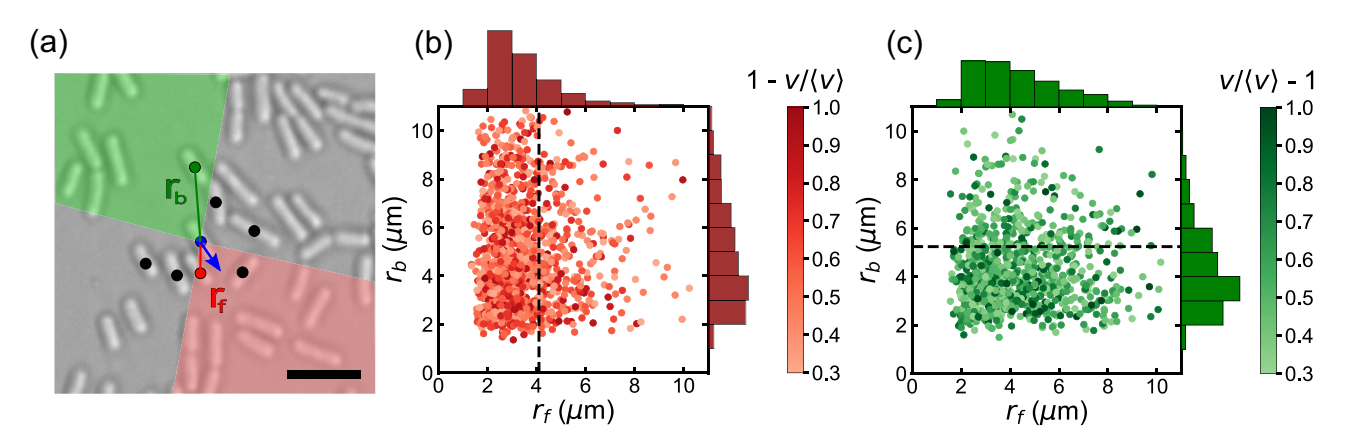


FIG. 4. Dependence of bacterial velocity on the relative positions of their neighbors in the 2D geometry. (a) The positions of the nearest neighbors of the reference bacterium marked by the blue arrow. The black, green and red dots denote the Voronoi nearest neighbors of the reference bacterium. Nearest neighbors are searched in the forward (pink shaded) region and the backward (green shaded) region, where each region lies within $\pm 45^{\circ}$ of the direction parallel or antiparallel to the swimming direction of the reference bacterium. The distance to the closest nearest neighbor in the forward region (a green dot) is r_f and the distance to the closest nearest neighbor in the backward region (a green dot) is r_b . (b) The distribution of r_f and r_b when bacterial velocity $v/\langle v\rangle < 0.7$. (c) The distribution of r_f and r_b when bacterial velocity $v/\langle v\rangle > 1.3$. The color bars represent the extent of deviation of the normalized velocity from the mean, quantified by $1 - v/\langle v\rangle$ in (b) and by $v/\langle v\rangle - 1$ in (c). A darker shade of color corresponds to a greater deviation from the mean velocity. The dashed black lines denote the 75th percentile of r_f in (b) and the 75th percentile of r_b in (c).

again confirms the collision-induced slowdown, essential for the formation of bacterial clusters. Quantitatively, we use the 75th percentiles of the distributions of r_f and r_b as representative measures of the forward nearest neighbor and backward nearest neighbor distances. The 75th percentiles of r_f and r_b for the slowdown events are $r_f^-=4.1~\mu\mathrm{m}$ and $r_b^-=6.3~\mu\mathrm{m}$, respectively. $r_f^- < r_b^-$, showing that a bacterium with the forward nearest neighbor closer than the backward nearest neighbor is more likely to experience a slowdown.

More interestingly, for the speedup events with $v/\langle v \rangle >$ 1.3, most data congregate around lower values of r_b with the 75th percentile being at $r_b^+ = 5.1 \ \mu \text{m}$ [Fig. 4(c)]. In comparison, the 75th percentile of r_f is larger at $r_f^+ = 5.6 \mu m$, a trend that is opposite to that of the slowdown events. Hence, a bacterium with the backward nearest neighbor closer than the forward nearest neighbor is more likely to experience a speedup. Moreover, $r_b^+ < r_b^-$, showing that the distance to the backward nearest neighbor in a speedup event is smaller than that in a slowdown event on average. Both of these results suggest that the presence of a backward neighbor at a short distance behind a bacterium enhances its swimming speed. Such an enhancement facilitates the quick dissolution of bacterial clusters after the removal of blockage, where bacteria in the front of a cluster accelerate to leave the cluster. The velocity enhancement due to backward neighbors is unique to swimming bacteria under Hele-Shaw confinement and has not been observed in swarming bacteria on agar surface [30] or in clustering microtubules [34] and actin filaments [35].

Why does a backward neighbor enhance the swimming speed of bacteria? *E. coli* cells swim due to the thrust force generated by the rotation of a flagellar bundle trailing behind the cell body [46,47]. We hypothesize that the presence of a neighboring cell body in a tightly confined geometry close to the flagella increases the thrust force [48], which causes an increase in the swimming speed. Thus, the interactions with its forward and backward neighbors strongly affect the swimming velocity of the bacterium in the 2D geometry, which in turn affects the structure of bacterial clusters. Each bacterium in a cluster has a different distribution of forward and backward nearest neighbors, resulting in a large variation of the swimming velocities of bacteria in the cluster. Thus, bacteria from the same cluster swim at different speeds, leading to the quick dissolution of the cluster.

E. Single bacterial dynamics in 2D and quasi-2D geometries

The qualitative difference in the emergent collective phases in the 2D and quasi-2D geometries also leads to a drastic difference in the swimming behavior of individual bacteria in these two geometries even at the same concentration. To highlight these differences, we compare the swimming trajectories at a high density of $\phi = 0.15$ and a high swimming velocity of $V = 13 \ \mu \text{m/s}$ in the 2D and quasi-2D geometries.

First, we compute the persistence of the swimming direction of individual bacteria in the two geometries. The persistence of the swimming direction of bacteria is quantified by the autocorrelation $C(t) = \langle \cos{(\alpha(t_0))} \cos{(\alpha(t_0 + t))} \rangle_{t_0}$, where the angle $\alpha(t)$ indicates the direction of the bacterial swimming at time t with respect to the x axis in the laboratory frame. C(t) decays faster in the 2D geometry than

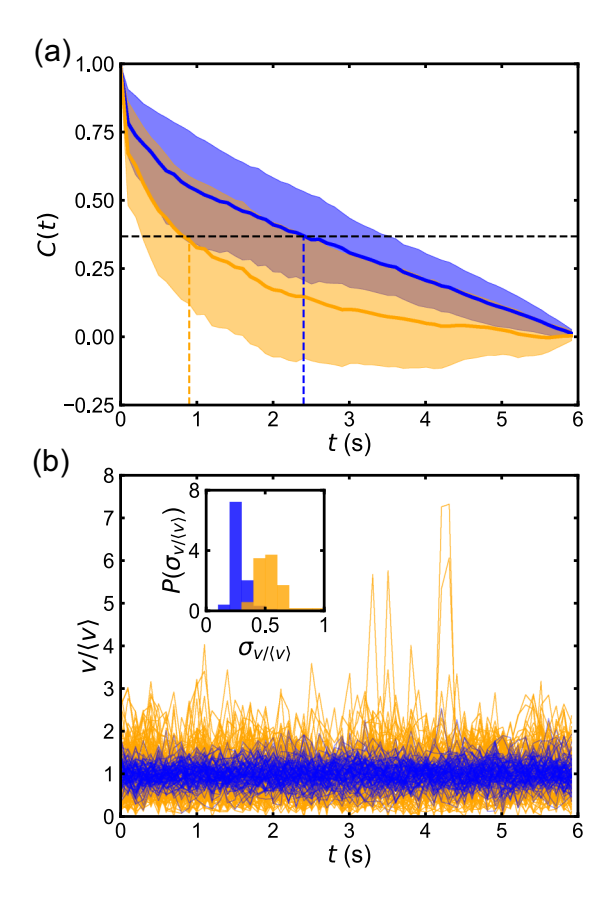


FIG. 5. Comparison of the swimming behaviors of bacteria in the 2D and quasi-2D geometries at the same bacterial area fraction of $\phi=0.15$. (a) The autocorrelation of the swimming direction of bacteria, C(t), for the 2D (gold) and quasi-2D (blue) geometries. The thick lines are the means calculated over 100 bacteria in the quasi-2D geometry and over 117 bacteria in the 2D geometry, whereas the shaded region represents one standard deviation around the means. The horizontal-dashed-black line corresponds to C(t)=1/e. The dashed gold- and blue-vertical lines indicate the persistence time of bacterial swimming $\tau=0.9$ s for the 2D geometry and $\tau=2.4$ s for the quasi-2D geometry, respectively. (b) The temporal evolution of the normalized velocity of individual bacteria, $v(t)/\langle v \rangle$, for the 2D (gold) and quasi-2D (blue) geometries. The inset shows the probability distributions of the standard deviation of $v/\langle v \rangle$ of different bacterial trajectories, $P(\sigma_{v/\langle v \rangle})$.

that in the quasi-2D geometry, implying a shorter persistence of the swimming bacteria in 2D [Fig. 5(a)]. The persistence time of bacterial swimming τ can be defined as the time at which C(t) decays to 1/e, where $e \approx 2.718$ is Euler's number. $\tau = 2.4 \pm 1.4$ s in quasi-2D, whereas it decreases by 60% in 2D at $\tau = 0.9 \pm 0.6$ s. The short persistence in 2D is a direct consequence of the noncrossing collisions and the many-body steric interactions. As bacteria are unable to cross over during collision, they must change their swimming directions frequently at high ϕ . In contrast, a bacterium in quasi-2D is able to cross over during collisions and maintain its swimming direction

Second, we also examine the temporal fluctuations of the velocity of individual bacteria in both geometries. Figure 5(b) shows the temporal variation of the normalized bacterial velocity $v(t)/\langle v \rangle$ in the 2D and quasi-2D geometries. The

velocity fluctuations in the 2D geometry are considerably stronger than those in the quasi-2D geometry. The velocity fluctuation of each bacteria can be quantified by the standard deviation of its normalized velocity, $\sigma_{v/\langle v \rangle}$, around the mean. Figure 5(b) inset shows the probability distributions of $\sigma_{v/\langle v \rangle}$ of all bacteria in the two different geometries. The average standard deviation of velocities is about 50% of the mean velocity in the 2D geometry, whereas it is only 25% of the mean in the quasi-2D geometry. This difference in velocity fluctuations can again be inferred from the strong many-body steric and near-field hydrodynamic interactions between the bacteria in the 2D geometry. A bacterium in 2D slows down instantaneously upon encountering a forward neighbor in its path and speeds up due to the presence of a backward neighbor close to it. At high densities, collisions between bacteria result in frequent speedups and slowdowns, contributing to the enhanced velocity fluctuations in the 2D geometry. In contrast, a bacterium in the quasi-2D geometry is able to slide past a neighbor in its path without significantly slowing down or speeding up, resulting in weak velocity fluctuations.

IV. DISCUSSION

Our experimental findings with confined swimming bacteria share a striking resemblance with recent experiments on the collective dynamics of molecular-motor-driven microtubules [34]. In the microtubule system, a long-range nematic order also emerges when individual microtubules are able to cross over each other during a collision, while a short-range polar order is observed when microtubules cannot cross over during a collision. This similarity suggests a universality of the collective behaviors in the two arguably most important examples of biological active matter [2]. Moreover, our experimental observations also complement recent numerical simulations of self-propelled rod-like particles where a nematic phase emerges when the particles are able to cross over each other [36,39–41], whereas the prevention of crossing over leads to the emergence of polar order [36,40,42–44].

It is worth noting that the propulsion mechanism of *E. coli* gives rise to complicated hydrodynamic effects, which are unique to our bacterial system and absent in the microtubule experiments and numerical simulations without hydrodynamic interactions. These nontrivial near-field hydrodynamic effects, when modified by geometric confinement, result in the enhanced velocity fluctuations and transient nature of bacterial clusters. Due to the absence of destabilizing hydrodynamic interactions, microtubule clusters at high densities are stable and long lived [49], and can dynamically merge together or split into smaller clusters [34,35,49]. Such dynamic processes are not observed in our experiments due to the short lifetimes of bacterial clusters.

Lastly, experiments on actomyosin motility assays showed qualitatively different trends in emergent collective dynamics. By increasing the bonding strength between actin filaments and substrates covered with myosin motors, which suppresses the ability of actin filaments in crossing over each other during a collision, Huber and coauthors observed a transition from a polar phase to a nematic phase [50], opposite to the trends of the confined bacterial and the microtubule systems. Such a different phase behavior may arise due to the different me-

chanical properties of active particles. Actin filaments have much higher aspect ratios than bacteria and are more flexible compared to either bacterial bodies or microtubules. It is an open question as to how the mechanical properties of active particles modify local interparticle interactions and determine the symmetry of collective dynamics.

In conclusion, our experiments reveal that a small change in the degree of confinement can qualitatively alter the collective swimming behaviors of bacteria. The critical gap thickness of the Hele-Shaw chamber, h_c , where the transition between the nematic and the cluster phase occurs, should be around twice the width of bacteria w_d at $2w_d \approx 2 \mu m$. The precise value of h_c is hard to assess a priori due to the natural variation in bacterial shapes and the complex interaction between bacteria and solid boundaries [7]. Furthermore, as the gap thickness at such a small scale is hard to control accurately, experiments with seemingly similar geometries may result in completely different emergent phases. Thus, our results help to resolve the contradictory findings of previous experiments [21,22]. Future work should be aimed at the construction of microfluidic devices of precisely controlled thicknesses to determine the critical gap thickness h_c . As the thickness of the Hele-Shaw chamber is increased further from the quasi-2D geometry to the bulk limit, we would expect the emergence of bacterial turbulence in bulk suspensions, where the long-range hydrodynamic interaction overcomes the steric interaction and dictates the collective swimming of bacteria [15]. The nature of the transition between the long-range nematic phase to bacterial turbulence upon increasing the gap thickness is an interesting direction for a future study. More broadly, the ability to control the emergent behaviors of active matter via geometric confinement provides not only a powerful method to probe the intrinsic dynamics of active matter in different dimensions but also a practical tool to tailor the behaviors of active systems in potential engineering applications.

ACKNOWLEDGMENTS

We are indebted to Shuo Guo for helping with the experiments and for providing valuable insights. We also thank Renan Gross and Oliver Meacock for helping with the code used for segmenting and tracking bacteria in 2D, and thank Robert Großmann, Shashank Kamdar, Zhengyang Liu, Yi Peng, Fernando Peruani and Xinliang Xu for helpful discussions. This work was funded by NSF CBET Grants No. 1702352 and No. 2028652 and the David and Lucile Packard Foundation. We dedicate this paper to the memory of our mentor and friend, Prof. James W. Swan.

APPENDIX A: METHODS

1. Bacterial strain and culturing

Wild-type *E. coli* (BW25113) are genetically modified to express the transmembrane proton pump proteorhodopsin (PR), using the plasmid pZE-PR encoding the SAR86 γ -proteobacterial PR-variant [51]. As the activity of PR is correlated with the intensity of incident light, we are able to control the swimming velocity of bacteria with light.

To prepare a suspension of motile bacteria, we inoculate a small amount of bacterial frozen stock in 2 mL Terrific Broth [tryptone 1.2% (w/v), yeast extract 2.4% (w/v) and glycerol 0.4% (w/v)]. Bacteria are then incubated at 37 °C for 15 hours in an orbital shaker operating at 250 rpm. This bacterial culture is then diluted 1:100 with fresh Terrific Broth and grown at 30 °C for 6.5 hours. We add 1 mM isopropyl β -d-1-thiogalactopyranoside and 10 μ M methanolic all-trans-retinal in the mid-log phase of bacterial growth, to trigger the expression of PR. Finally, in the late log phase, bacteria are harvested by gentle centrifugation. The supernatant is discarded, and the bacteria are then resuspended in deionized water. The suspension is further washed twice and adjusted by adding water to reach the desired concentration.

2. Hele-Shaw chamber

To create a Hele-Shaw chamber, we first deposit a droplet of E. coli suspension of controlled volume on a glass slide. The droplet is then confined by gently pressing a glass coverslip of dimensions 18 mm by 18 mm onto it, ensuring the complete absence of air bubbles in the confined droplet. The edges of the coverslip are then sealed with UV-curable adhesive. We have confirmed that the short exposure of lowdose UV radiation for curing does not affect the motility of bacteria. Note that the motility of the light-control bacteria is driven by the incident light and does not require oxygen in the confined chamber. The swimming speeds of bacteria do not decline during the course of a typical experiment over 10 minutes. The thickness of the Hele-Shaw chamber is controlled by changing the volume of the confined droplet. 0.7 μ L droplets are used for the 2D geometry, which give a gap thickness about 2.2 μ m. 0.9 μ L droplets are used for the quasi-2D geometry, which give a gap thickness about 2.8 μ m.

3. Video microscopy

The dynamics of bacteria in Hele-Shaw chambers are imaged through an inverted bright-field microscope (Nikon Ti-Eclipse) using a $60\times$ objective lens with a numerical aperture of 1.25. The field of view is set at 2320 pixels by 2080 pixels, which corresponds to a physical dimension of 251 μ m by 225 μ m. The swimming velocity of bacteria is controlled by changing the light intensity of the illumination lamp of the bright-field microscope. We first prepare Hele-Shaw chambers containing different concentrations of bacteria. The light intensity is then varied to adjust the swimming speed of bacteria. The resultant emergent phase behavior is finally imaged. Videos are recorded at a frame rate of 30 frames per second (fps) for a total of 1000 frames using a scientific complementary metal-oxide-semiconductor (sCMOS) camera (Andor Zyla 4.2).

4. Image processing and analysis

The acquired videos are first preprocessed using customwritten MATLAB and Python scripts to remove background noise. The images are then binarized using Otsu's method, where bacterial cells appear as white blobs in the image. The software package developed by Be'er *et al.* [23] is used to segment the bacterial cells. The area fraction occupied by

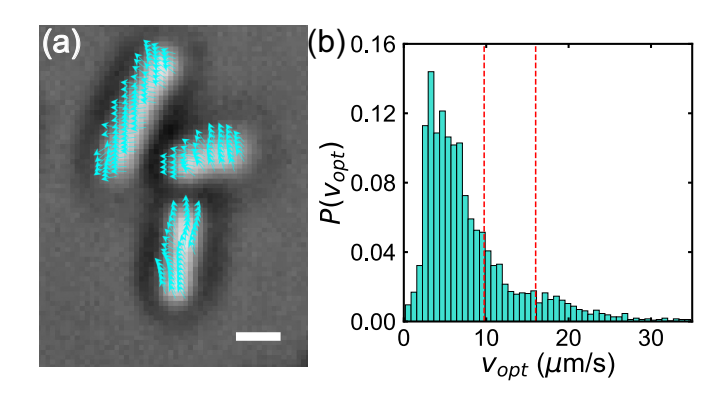


FIG. 6. Method of optical flow for bacterial velocity measurements. (a) The directions of the velocity field $v_{\rm opt}$ for 3 different bacteria. The scale bar is 1 μ m. Only one out of every 16 velocity vectors has been shown for clarity. (b) Probability density of the magnitude of $v_{\rm opt}$ for a single bacterium. The red dashed lines represent the 75th and 90th percentiles of the distribution.

bacteria in an image is defined as the ratio of the number of white pixels to the total number of pixels. The positions \mathbf{r} and the orientations θ of these white blobs in the image, representing bacteria, are then extracted.

In the 2D geometry, bacteria cannot overlap or cross over each other. Hence, all the bacteria in the field of view can be accurately tracked. To determine the instantaneous velocities of bacteria in the 2D geometry, the FAST module developed by Meacock et al. is used [52]. The velocities thus obtained lie within 10% of that measured by direct manual tracking. In the quasi-2D geometry, bacteria can cross over each other, making it difficult to track them from one frame to the next. To determine their instantaneous velocities in the quasi-2D geometry, we use the principle of optical flow [53,54]. After smoothing the images with a Gaussian filter, the Farnebäck dense optical flow method [55] is used to calculate the velocity field of all pixels between two consecutive frames of a video. Next, we consider the velocity vectors v_{opt} of white pixels in the binary image representing bacterial bodies. The directions of $v_{\rm opt}$ obtained for 3 different bacterial cells are illustrated in Fig. 6(a). The distribution of the magnitudes of v_{opt} is shown in Fig. 6(b). As the contrast gradient between the pixels denoting a cell body and those denoting the background is highest at the edge of the cell, $v_{\rm opt}$ obtained from the pixels close to the edge of the cell most accurately reflects the speed of the cell. Thus, the tail of the distribution of v_{opt} can be averaged to estimate the true swimming velocity of a bacterial cell [54]. We find that the mean of $v_{\rm opt}$ calculated between the 75th and 90th percentile range [red dotted lines in Fig. 6(b)] lies within 10% of the velocity obtained using direct manual tracking in our experiments. Thus, the method of optical flow provides a reliable estimate of the swimming velocity of bacteria in the quasi-2D geometry, circumventing the challenges faced with respect to bacteria going out of the plane in standard particle tracking velocimetry.

For each frame in the videos, we determine the area fraction, the velocity of bacteria and the nematic order parameter in case of the quasi-2D geometry, and the number of clusters in case of the 2D geometry. These values are then averaged

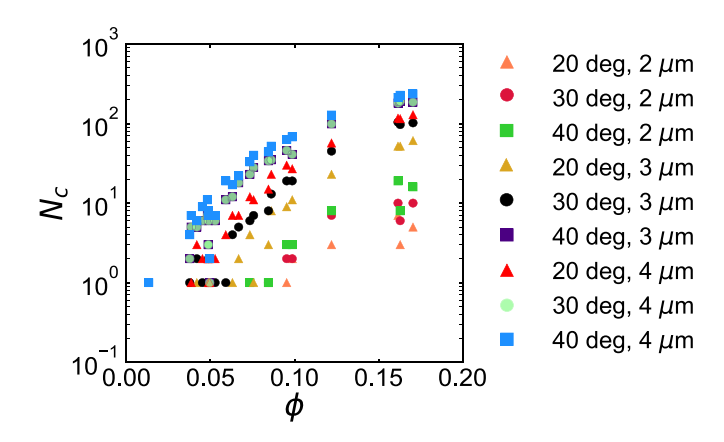


FIG. 7. Number of bacterial clusters as a function of area fraction ϕ for different cut-off angles $\Delta\theta$ and cut-off distances Δr . The ensemble average velocities of bacteria V are fixed between 8 μ m/s and 10 μ m/s.

over the 1000 frames of a video to give ϕ , V, S, and N_c reported in the main text.

To obtain long-time statistics of trajectories and calibrate our tracking algorithms, we also manually track bacteria for both the 2D and quasi-2D geometries at $\phi=0.15$ and $V=13~\mu m/s$ at a frame rate of 10 frames per second for 6 seconds. For the nematic phase, we track the motion of a total of 100 bacteria, whose trajectories are shown in Fig. 1(b). For the cluster phase, we first identify 17 different bacterial clusters and then track a total of 117 bacteria in these clusters. The bacterial trajectories are shown in Fig. 1(e). The trajectories of the bacteria in 2D are used to calculate the time dependence of the adjacent angles and pairwise distances in clusters (Fig. 3), and the neighbor dependence of bacterial velocities (Fig. 4). Trajectories from both geometries are used to calculate the directional persistence [Fig. 5(a)] and the velocity fluctuations [Fig. 5(b)].

5. Cluster identification

Following the convention of previous studies [30,32], we define bacterial clusters using a cut-off distance $\Delta r = 3 \mu m$

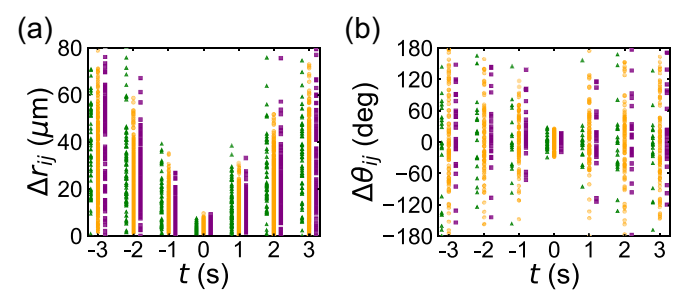


FIG. 9. Dynamics of bacterial clusters at different area fractions ϕ . (a) Δr_{ij} and (b) $\Delta \theta_{ij}$ for $\phi=0.09$ (green triangles), $\phi=0.15$ (gold circles), and $\phi=0.19$ (purple squares). The data have been obtained for 17 different clusters for $\phi=0.15$, and 5 different clusters each for $\phi=0.09$ and $\phi=0.19$.

and a cut-off angle $\Delta\theta=30^\circ$. Nevertheless, the qualitative features of the 2D phase diagram in Fig. 1(f) do not change when we vary Δr and $\Delta\theta$ around the chosen values within a reasonable range. Figure 7 shows the number of clusters N_c versus ϕ for different choices of Δr and $\Delta\theta$ around $\Delta r=3~\mu{\rm m}$ and $\Delta\theta=30^\circ$ with the ensemble average velocity of bacteria V between 8 $\mu{\rm m/s}$ and 10 $\mu{\rm m/s}$.

APPENDIX B: SUPPORTING DATA

1. Incoming and outgoing angles

Figure 8(a) shows the scatter plot of the incoming angle β_{in} versus the outgoing angle β_{out} used for the construction of Fig. 2(g). Each data point in Fig. 8(a) represents an experimentally observed collision event. The total number of collisions analyzed for the quasi-2D geometry is 1,119, whereas the total number of collisions analyzed for the 2D geometry is 1,287. The statistics adopted here are comparable to previous measurements on the same quantities [21,45,50]. The large standard deviations of β_{out} shown in Fig. 2(g) and Fig. 8(a) arise from the natural variation of the outgoing swimming directions of bacteria, suggesting the weak nematic alignment induced by individual binary collisions.

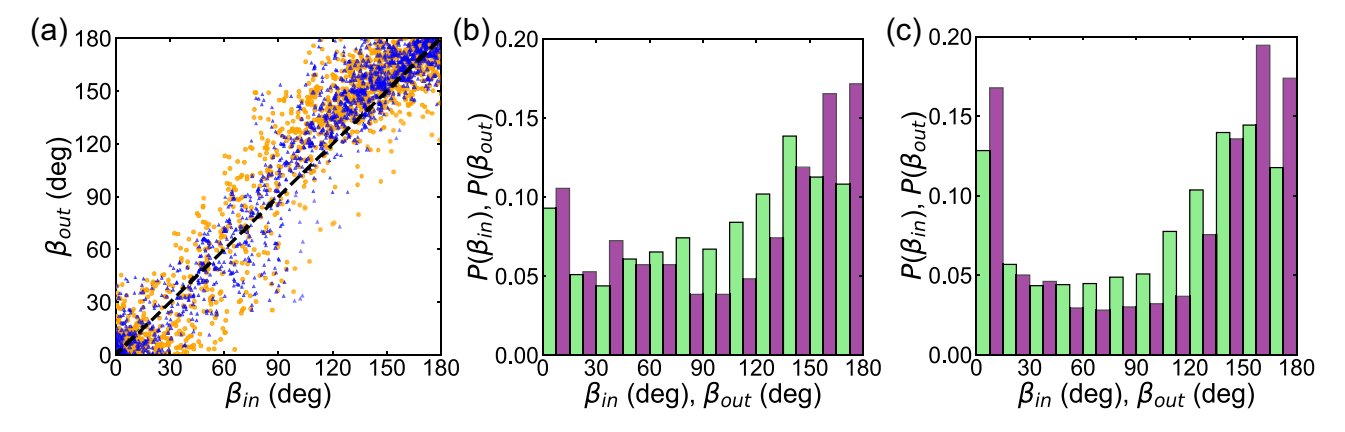


FIG. 8. Statistics of binary collisions. (a) Scatter plot showing the distributions of incoming angle β_{in} and outgoing angle β_{out} for the quasi-2D (blue triangles) and 2D (gold circles) geometries. The black-dashed line represents the condition $\beta_{in} = \beta_{out}$, corresponding to collisions without any alignment. (b) The probability distributions of β_{in} (green) and β_{out} (purple) in the quasi-2D geometry. (c) The probability distributions of β_{in} (green) and β_{out} (purple) in the 2D geometry.

Figures 8(b) and 8(c) further show the probability distributions of $\beta_{\rm in}$ and $\beta_{\rm out}$ for the quasi-2D and 2D geometries, respectively. The number of collisions with $\beta_{\rm in} > 90^{\circ}$ is larger than that with $\beta_{\rm in} < 90^{\circ}$. This is consistent with the observation of Nishiguchi *et al.* [21], who reasoned that a collision between a pair of bacteria with an acute $\beta_{\rm in}$ lasts longer due to similar outgoing directions. Such a configuration increases the probability of encountering a third bacterium, which prevents the collision from being binary. Furthermore, under 2D confinement, a pair of bacteria are hydrodynamically bound and swim parallel with their bodies side by side [33], which may explain the abundance of coswimming bacteria with $\beta_{\rm in} \approx 0^{\circ}$.

2. Density dependence of clustering dynamics

To examine the effect of bacterial density on the dynamics of clustering, we measure the temporal variation of the pairwise distances Δr_{ij} and the difference in adjacent angles $\Delta \theta_{ij}$ of bacteria in clusters at $\phi=0.09$ and $\phi=0.19$ and compare the results with those at $\phi=0.15$ shown in Fig. 3. For each of these two additional area fractions, five different clusters are sampled from two independent experimental runs. Each of the clusters contains 4–7 bacteria. The clustering dynamics at different area fractions show quantitatively similar trends (Fig. 9).

- [1] S. Ramaswamy, The mechanics and statistics of active matter, Annu. Rev. Condens. Matter Phys. 1, 323 (2010).
- [2] M. C. Marchetti, J.-F. Joanny, S. Ramaswamy, T. B. Liverpool, J. Prost, M. Rao, and R. A. Simha, Hydrodynamics of soft active matter, Rev. Mod. Phys. 85, 1143 (2013).
- [3] J. Schwarz-Linek, J. Arlt, A. Jepson, A. Dawson, T. Vissers, D. Miroli, T. Pilizota, V. A. Martinez, and W. C. Poon, *Escherichia coli* as a model active colloid: A practical introduction, Colloids and Surfaces B: Biointerfaces 137, 2 (2016).
- [4] A. Be'er and G. Ariel, A statistical physics view of swarming bacteria, Mov. Ecol. 7, 9 (2019).
- [5] H. M. López, J. Gachelin, C. Douarche, H. Auradou, and E. Clément, Turning Bacteria Suspensions into Superfluids, Phys. Rev. Lett. 115, 028301 (2015).
- [6] Y. Peng, L. Lai, Y.-S. Tai, K. Zhang, X. Xu, and X. Cheng, Diffusion of Ellipsoids in Bacterial Suspensions, Phys. Rev. Lett. 116, 068303 (2016).
- [7] J. C. Conrad and R. Poling-Skutvik, Confined flow: Consequences and implications for bacteria and biofilms, Annu. Rev. Chem. Biomol. Eng. 9, 175 (2018).
- [8] L. Ranjard and A. Richaume, Quantitative and qualitative microscale distribution of bacteria in soil, Res. Microbiol. 152, 707 (2001).
- [9] T. Bhattacharjee and S. S. Datta, Bacterial hopping and trapping in porous media, Nat. Commun. 10, 2075 (2019).
- [10] V. Ki and C. Rotstein, Bacterial skin and soft tissue infections in adults: a review of their epidemiology, pathogenesis, diagnosis, treatment and site of care, Can. J. Infect. Dis. Med. Microbiol. 19, 173 (2008).
- [11] C. Dombrowski, L. Cisneros, S. Chatkaew, R. E. Goldstein, and J. O. Kessler, Self-Concentration and Large-Scale Coherence in Bacterial Dynamics, Phys. Rev. Lett. 93, 098103 (2004).
- [12] A. Sokolov, R. E. Goldstein, F. I. Feldchtein, and I. S. Aranson, Enhanced mixing and spatial instability in concentrated bacterial suspensions, Phys. Rev. E 80, 031903 (2009).
- [13] H. H. Wensink, J. Dunkel, S. Heidenreich, K. Drescher, R. E. Goldstein, H. Löwen, and J. M. Yeomans, Meso-scale turbulence in living fluids, Proc. Natl. Acad. Sci. USA 109, 14308 (2012).
- [14] S. Guo, D. Samanta, Y. Peng, X. Xu, and X. Cheng, Symmetric shear banding and swarming vortices in bacterial superfluids, Proc. Natl. Acad. Sci. USA 115, 7212 (2018).
- [15] Y. Peng, Z. Liu, and X. Cheng, Imaging the emergence of bacterial turbulence: Phase diagram and transition kinetics, Sci. Adv. 7, eabd1240 (2021).

- [16] Z. Liu, W. Zeng, X. Ma, and X. Cheng, Density fluctuations and energy spectra of 3D bacterial suspensions, Soft Matter 17, 10806 (2021).
- [17] T. Brotto, J.-B. Caussin, E. Lauga, and D. Bartolo, Hydrodynamics of Confined Active Fluids, Phys. Rev. Lett. 110, 038101 (2013).
- [18] A. C. H. Tsang and E. Kanso, Flagella-induced transitions in the collective behavior of confined microswimmers, Phys. Rev. E 90, 021001(R) (2014).
- [19] I. S. Aranson, A. Sokolov, J. O. Kessler, and R. E. Goldstein, Model for dynamical coherence in thin films of self-propelled microorganisms, Phys. Rev. E 75, 040901(R) (2007).
- [20] A. Baskaran and M. C. Marchetti, Nonequilibrium statistical mechanics of self-propelled hard rods, J. Stat. Mech.: Theory Exp. (2010) P04019.
- [21] D. Nishiguchi, K. H. Nagai, H. Chaté, and M. Sano, Long-range nematic order and anomalous fluctuations in suspensions of swimming filamentous bacteria, Phys. Rev. E 95, 020601(R) (2017).
- [22] J.-M. Swiecicki, O. Sliusarenko, and D. B. Weibel, From swimming to swarming: *Escherichia coli* cell motility in two-dimensions, Integr. Biol. 5, 1490 (2013).
- [23] A. Be'er, B. Ilkanaiv, R. Gross, D. B. Kearns, S. Heidenreich, M. Bär, and G. Ariel, A phase diagram for bacterial swarming, Commun. Phys. 3, 66 (2020).
- [24] H. Wioland, F. G. Woodhouse, J. Dunkel, J. O. Kessler, and R. E. Goldstein, Confinement Stabilizes a Bacterial Suspension into a Spiral Vortex, Phys. Rev. Lett. 110, 268102 (2013).
- [25] E. Lushi, H. Wioland, and R. E. Goldstein, Fluid flows created by swimming bacteria drive self-organization in confined suspensions, Proc. Natl. Acad. Sci. USA 111, 9733 (2014).
- [26] H. Wioland, E. Lushi, and R. E. Goldstein, Directed collective motion of bacteria under channel confinement, New J. Phys. 18, 075002 (2016).
- [27] Z. Liu, K. Zhang, and X. Cheng, Rheology of bacterial suspensions under confinement, Rheol. Acta 58, 439 (2019).
- [28] Y. Wu, Collective motion of bacteria in two dimensions, Quant. Biol. 3, 199 (2015).
- [29] D. B. Kearns, A field guide to bacterial swarming motility, Nat. Rev. Microbiol. **8**, 634 (2010).
- [30] H.-P. Zhang, A. Beer, E.-L. Florin, and H. L. Swinney, Collective motion and density fluctuations in bacterial colonies, Proc. Natl. Acad. Sci. USA 107, 13626 (2010).
- [31] See Supplemental Material at http://link.aps.org/supplemental/ 10.1103/PhysRevResearch.4.023105 for Movies 1 and 2.

- [32] Y. Yang, V. Marceau, and G. Gompper, Swarm behavior of self-propelled rods and swimming flagella, Phys. Rev. E 82, 031904 (2010).
- [33] Y. Li, H. Zhai, S. Sanchez, D. B. Kearns, and Y. Wu, Noncontact Cohesive Swimming of Bacteria in Two-Dimensional Liquid Films, Phys. Rev. Lett. 119, 018101 (2017).
- [34] S. Tanida, K. Furuta, K. Nishikawa, T. Hiraiwa, H. Kojima, K. Oiwa, and M. Sano, Gliding filament system giving both global orientational order and clusters in collective motion, Phys. Rev. E 101, 032607 (2020).
- [35] A. Sciortino and A. R. Bausch, Pattern formation and polarity sorting of driven actin filaments on lipid membranes, Proc. Natl. Acad. Sci. USA 118, e2017047118 (2021).
- [36] R. Großmann, I. S. Aranson, and F. Peruani, A particle-field approach bridges phase separation and collective motion in active matter, Nat. Commun. 11, 5365 (2020).
- [37] J. Denk and E. Frey, Pattern-induced local symmetry breaking in active-matter systems, Proc. Natl. Acad. Sci. USA 117, 31623 (2020).
- [38] M. Bär, R. Großmann, S. Heidenreich, and F. Peruani, Selfpropelled rods: Insights and perspectives for active matter, Annu. Rev. Condens. Matter Phys. 11, 441 (2020).
- [39] F. Ginelli, F. Peruani, M. Bär, and H. Chaté, Large-Scale Collective Properties of Self-Propelled Rods, Phys. Rev. Lett. 104, 184502 (2010).
- [40] X.-q. Shi and H. Chaté, Self-propelled rods: Linking alignment-dominated and repulsion-dominated active matter, arXiv:1807.00294.
- [41] F. Peruani, A. Deutsch, and M. Bär, A mean-field theory for self-propelled particles interacting by velocity alignment mechanisms, Eur. Phys. J.: Spec. Top. 157, 111 (2008).
- [42] F. Peruani, A. Deutsch, and M. Bär, Nonequilibrium clustering of self-propelled rods, Phys. Rev. E **74**, 030904(R) (2006).
- [43] M. Abkenar, K. Marx, T. Auth, and G. Gompper, Collective behavior of penetrable self-propelled rods in two dimensions, Phys. Rev. E **88**, 062314 (2013).

- [44] S. Weitz, A. Deutsch, and F. Peruani, Self-propelled rods exhibit a phase-separated state characterized by the presence of active stresses and the ejection of polar clusters, Phys. Rev. E 92, 012322 (2015).
- [45] R. Suzuki, C. A. Weber, E. Frey, and A. R. Bausch, Polar pattern formation in driven filament systems requires non-binary particle collisions, Nat. Phys. 11, 839 (2015).
- [46] H. C. Berg, E. coli in Motion (Springer, New York, 2004).
- [47] S. Kamdar, S. Shin, P. Leishangthem, L. F. Francis, X. Xu, and X. Cheng, The colloidal nature of complex fluids enhances bacterial motility, Nature (London) **603**, 819 (2022).
- [48] G. Vizsnyiczai, G. Frangipane, S. Bianchi, F. Saglimbeni, D. DellArciprete, and R. Di Leonardo, A transition to stable one-dimensional swimming enhances *E. coli* motility through narrow channels, Nat. Commun. 11, 2340 (2020).
- [49] R. Suzuki and A. R. Bausch, The emergence and transient behaviour of collective motion in active filament systems, Nat. Commun. 8, 41 (2017).
- [50] L. Huber, R. Suzuki, T. Krüger, E. Frey, and A. Bausch, Emergence of coexisting ordered states in active matter systems, Science 361, 255 (2018).
- [51] J. M. Walter, D. Greenfield, C. Bustamante, and J. Liphardt, Light-powering *Escherichia coli* with proteorhodopsin, Proc. Natl. Acad. Sci. USA 104, 2408 (2007).
- [52] O. J. Meacock, A. Doostmohammadi, K. R. Foster, J. M. Yeomans, and W. M. Durham, Bacteria solve the problem of crowding by moving slowly, Nat. Phys. 17, 205 (2021).
- [53] A. Rabani, G. Ariel, and A. Be'er, Collective motion of spherical bacteria, PLoS One 8, e83760 (2013).
- [54] H. Jeckel, E. Jelli, R. Hartmann, P. K. Singh, R. Mok, J. F. Totz, L. Vidakovic, B. Eckhardt, J. Dunkel, and K. Drescher, Learning the space-time phase diagram of bacterial swarm expansion, Proc. Natl. Acad. Sci. USA 116, 1489 (2019).
- [55] G. Farnebäck, Two-frame motion estimation based on polynomial expansion, in *Scandinavian Conference on Image Analysis* (Springer, Berlin, 2003), pp. 363–370.